

# Analytical Methods

Accepted Manuscript



This is an *Accepted Manuscript*, which has been through the Royal Society of Chemistry peer review process and has been accepted for publication.

*Accepted Manuscripts* are published online shortly after acceptance, before technical editing, formatting and proof reading. Using this free service, authors can make their results available to the community, in citable form, before we publish the edited article. We will replace this *Accepted Manuscript* with the edited and formatted *Advance Article* as soon as it is available.

You can find more information about *Accepted Manuscripts* in the [Information for Authors](#).

Please note that technical editing may introduce minor changes to the text and/or graphics, which may alter content. The journal's standard [Terms & Conditions](#) and the [Ethical guidelines](#) still apply. In no event shall the Royal Society of Chemistry be held responsible for any errors or omissions in this *Accepted Manuscript* or any consequences arising from the use of any information it contains.



## Analytical Methods

## PAPER

## Graphene quantum dots-decorated mesoporous silica nanoparticles for high aspirin loading capacity and its pH-triggered release

Received 00th January 20xx,  
Accepted 00th January 20xx

DOI: 10.1039/x0xx00000x

www.rsc.org/

Shaping Huang,<sup>a</sup> Liping Song,<sup>a</sup> Zhidong Xiao,<sup>ab\*</sup> Yue Hu,<sup>a</sup> Meiwen Peng,<sup>a</sup> Jinquan Li,<sup>b</sup> Xinsheng Zheng,<sup>a</sup> Bin Wu<sup>b</sup> and Chao Yuan<sup>a</sup>

In this paper, fluorescent graphene quantum dots (GQDs) grafted on the surface of mesoporous silica nanoparticles (MSN) vehicle were prepared and characterized. The as-prepared graphene quantum dots-decorated mesoporous silica nanoparticles (GQDs-MSN) exhibited excellent luminescence properties *in vitro*. Interestingly, compared to pure MSN, the specific surface area and pore volume of GQDs-MSN increased 59.1% and 48.9%, respectively. These optimized features granted GQDs-MSN high aspirin loading capability (mg/mg) that doubled pure MSN loading. Moreover, most of aspirin encapsulated (95.15%) could release from the surface of GQDs-MSN under acidic condition (pH 2.5) within 33 h.

### 1 Introduction

Mesoporous silica nanoparticles (MSN) have been studied extensively as drug carrier system due to their unparalleled structural characteristics and superior properties such as large specific surface area, uniform mesopores, excellent reactive surface, physicochemical stability, cytomembrane-penetrating ability, and high level biocompatibility.<sup>1-4</sup> It is crucial to real-time monitor the drug carrier MSN in living organism in order to guarantee targeting drug delivery. Notwithstanding those advantages, MSN itself cannot emit real-time signals to allow for the rapid detection and consequently follow the dynamic drug migratory route. Hence, efforts are focusing on how to enable the MSN to emit measurable signals once the drug released. One solution is to conjugate MSN with fluorescence materials such as semiconductor quantum dots (QDs), organic fluorescent dyes, or upconversion nanoparticles, which can be encapsulated into MSN and maintain their easily detectable characteristics in living organisms and cells.<sup>5-8</sup> However, the known toxicity, potential environmental hazard and chemical instability associated with these materials may limit their applications. For example, organic fluorescent dyes and upconversion nanoparticles are readily aggregate in aqueous environments, hence reduce their conjugation efficiency with MSN.<sup>9,10</sup> QDs-related biological applications would be restricted as a result of potential toxicity given the fact that the concurrent leakage of constituents metal cadmium and

selenium in QD core metalloid complex is hardly evitable.<sup>11-14</sup> Therefore, exploring benign fluorescent material with strong fluorescence, stable photophysical and chemical stability, low cytotoxicity, good biocompatibility and easily assembled is demanded.

Graphene, a two-dimensional atomic crystal reported by Geim and Novoselov more than a decade ago,<sup>15</sup> is considerably investigated owing to its novel physical properties, chemical modulatability<sup>16</sup> and potential applications in nanocomposite materials.<sup>17</sup> Graphene quantum dots (GQDs) have drawn great attentions in the past few years.<sup>18,19</sup> For example, GQDs-based blends synthesized by blending GQDs with conjugated poly(3-hexylthiophene-2,5-diyl) or poly(2-methoxy-5-(2-ethylhexyloxy)-1,4-phenylenevinylene) acceptors exhibits a significant enhancement in organic photovoltage characteristics by comparison with the corresponding conjugated polymer-graphene sheet ones.<sup>20</sup> GQDs have been also widely used in analytical chemistry and cell imaging.<sup>21,22</sup> For example, nitrogen-doped GQDs can achieve a large imaging depth of 1800  $\mu\text{m}$  that far surpasses the fundamental two-photon imaging depth limit.<sup>23</sup> However, the fluorescent GQDs have not been used for the construction of pH-triggered drug delivery system. Herein, for the first time, GQDs-MSN drug carrier system was designed by attaching fluorescent GQDs on the surface of MSN through electrostatic interaction, and aspirin was chosen to evaluate performance of our system in question. Briefly, GQDs-MSN exhibited excellent luminescence properties *in vitro*. By comparison with pure MSN, the specific surface area and pore volume of the as-prepared GQDs-MSN achieved 640.82  $\text{m}^2/\text{g}$  and 0.70  $\text{cm}^3/\text{g}$ , which lead to 59.1% and 48.9% increase, respectively. Most importantly, the aspirin loading capacity of the GQDs-MSN could reach 36.59%, which was twice as much as that of pure MSN (18.26%). Moreover, it is found that the majority of

<sup>a</sup> Department of Chemistry, College of Science, Huazhong Agricultural University, Wuhan 430070, P. R. China.

<sup>b</sup> State Key Laboratory of Agricultural Microbiology, Huazhong Agricultural University, Wuhan 430070, P. R. China.  
E-mail: zhidongxiao@mail.hzau.edu.cn; Fax: +86-27-87282048; Tel: +86-27-87286893.

aspirin (95.15%) loaded could release from the surface of GQDs-MSN at pH of 2.5 within 33 h, indicating the potential pH-triggered drug controlled release property of the GQDs-MSN and its clinical application.

## 2 Experimental

### 2.1 Chemicals

Potassium permanganate (KMnO<sub>4</sub>, A.R.), potassium nitrate (KNO<sub>3</sub>, A.R.), sulfuric acid (H<sub>2</sub>SO<sub>4</sub>, 98%), N-Cetyltrimethylammonium bromide (CTAB, A.R.), Ethanol (EtOH, A.R.), methyl alcohol (MeOH, A.R.), hydrochloric acid (HCl, 35.0-38.0%), sodium hydroxide (NaOH, A.R.), Ammonia (NH<sub>3</sub>·H<sub>2</sub>O, 28.0-30.0%), hydrogen peroxide (H<sub>2</sub>O<sub>2</sub>, 30wt%), tetraethylorthosilicate (TEOS, A.R.), N, N-dimethylformamide (DMF, A.R.), disodiumhydrogenphosphate (Na<sub>2</sub>HPO<sub>4</sub>, A.R.), sodium dihydrogen phosphate (NaH<sub>2</sub>PO<sub>4</sub>, A.R.), and monopotassiumphosphate (KH<sub>2</sub>PO<sub>4</sub>, A.R.) were purchased from Sinopharm Chemical Reagent Co., Ltd, China. (3-aminopropyl) triethoxysilane (APTES, 99%) and acetylsalicylic acid (aspirin, B.R.) were purchased from Aladdin Industrial Corporation, China. Graphite powder was purchased from Sigma-Aldrich. All the reagents were used as received without further purification. Dialysis bag (retained molecular weight: 3500 Da) was purchased from BIOSHARP. Water throughout all experiments was obtained by using a Milli-Q water system (18 MΩ).

### 2.2 Synthesis of GQDs

Graphene oxide (GO) was prepared from natural graphite powder according to a modified method.<sup>24</sup> Graphite (2 g) powders and KNO<sub>3</sub> (1 g) were added to 100 mL of 98% H<sub>2</sub>SO<sub>4</sub> at 0 °C (ice bath). Then 15 g of KMnO<sub>4</sub> was added gradually into GO dispersion with stirring and cooling so that the temperature of the mixture did not exceed 20 °C. The mixture was then maintained at 40 °C for 24 h. Thereafter deionized water (50 mL) was gradually added, causing an increase of temperature to 98 °C. After cooling to room temperature, the reaction mixture was diluted with 250 mL of deionized water, followed by the addition of 10 mL 30wt% H<sub>2</sub>O<sub>2</sub> until there was no bubble produced. The solution was centrifuged and washed with deionized water until the supernatant was neutral. The residue was dialyzed until no precipitate of BaSO<sub>4</sub> was observed upon the addition of a few drops of BaCl<sub>2</sub> solution to the dialysate in the container. The obtained dialysate was then ultrasonicated for 24 h, and then subjected to 10 min of centrifugation at 3000 rpm to remove the unexfoliated GO particles. In the end, the obtained GO was freeze-dried for 2 days.

GQDs were synthesized from GO according to previously reported method.<sup>25</sup> The as-prepared GO (150 mg) was dissolved in DMF (17 mL), and was dispersed into a homogeneous solution using an ultrasonic cell crusher within 30 min. Later on the solution was transferred into a poly (tetrafluoroethylene) Teflon-lined autoclave (50 mL) and heated at 200 °C for 5 h. The obtained liquid was centrifuged

to collect the brown transparent suspension. The solvent of the GQDs suspension was removed with a rotary evaporator, afterwards the solid product was suspended in deionized water. The mixture solution was further dialyzed in a dialysis bag (retained molecular weight: 3500 Da) and a yellowish-brown fluorescent GQDs suspension was obtained.

### 2.3 Synthesis of NH<sub>2</sub> group-modified MSN (MSN-NH<sub>2</sub>)

MSN-NH<sub>2</sub> was prepared using a one-pot method. CTAB (0.1 g), deionized water (25 mL), NH<sub>3</sub>·H<sub>2</sub>O (0.2 mL) and Ethanol (4 mL) were loaded into a one-neck flask and the mixture was vigorously stirred for 30 min at 40 °C. Then TEOS (0.5 mL) was added into the above solution, followed by the addition of 0.1 mL of APTES and the resulting mixture was stirred for another 12 h. Subsequently, the precipitate was collected by centrifugation and washed with water and ethanol for five times, and then dried in the vacuum oven at 80 °C overnight. Finally, CTAB and other organic components in the as-prepared precipitate were removed by extraction with MeOH and HCl mixtures. The as-prepared precipitate (0.25 g) was suspended in methanol (25 mL) and hydrochloric acid (2.5 mL), and stirred for 6 h at 60 °C. The product was collected by centrifugation, washed with methanol and dried at 80 °C.

### 2.4 Synthesis of GQDs-MSN

For the preparation of GQDs-MSN, the as-prepared MSN-NH<sub>2</sub> (50 mg) were dispersed in 10 mL the prepared GQDs aqueous solution (0.4 mg/mL) and ultrasonically (500 W) mixed for 30 min, then stirred overnight at room temperature, followed by stewing for 12 h. Finally, the solution was ultracentrifuged and the precipitates were washed with deionized water and ethanol for five times, and then dried in draught drying cabinet for 12 h at 80 °C.

### 2.5 Aspirin loading and release performances of GQDs-MSN

The adsorption of aspirin *in vitro* experiment was conducted as follows: 500 mg of GQDs-MSN was added into 100 mL of 5 mg/mL aspirin ethanol solution. The mixture in a sealed vial was first ultrasonicated for 30 min and then stirred at 200 rpm for 24 h at room temperature. Then the solution was ultracentrifuged at 15000 rpm for 1 h. The aspirin concentration in the supernatant was measured using a standard aspirin concentration curve generated with an UV-vis spectrophotometer at the wavelength of 276 nm from a series of aspirin solutions with different concentrations.

The drug loading capacity (LC) of GQDs-MSN was calculated formulas according to:

$$LC\% = A/B \times 100\% \quad (1)$$

Where A = the weight of aspirin; B = the weight of GQDs-MSN.

The release behavior of aspirin on GQDs-MSN was investigated by dialysis. Typically, aspirin-loaded GQDs-MSN (100 mg) was redispersed in 10 mL phosphate-buffer saline (PBS) solutions with pH 2.5, 7.4 and 9.0, respectively. Subsequently, all of them were transferred into dialysis bags, and the three bags were immersed into 190 mL of the corresponding PBS solution at 37 °C and stirred at 200 rpm.

The drug release was assumed to start now that the dialysis bags were placed into the reservoir. At fixed time intervals, 4 mL of the dialysis solution was removed for analysis and the same amount of PBS was added to keep the total volume unchanged. The extracted medium was analyzed by UV-vis spectrophotometer at the wavelength of 295.5 nm.

Calculation of the corrected concentration of the released aspirin is based on the equation:

$$Q_n = C_n V_0 + (C_1 + C_2 + \dots + C_{n-1})V \quad (2)$$

Where  $Q_n$  is the amount of the cumulative release of drug at the  $n$ th sampling point,  $C_n$  is the apparent concentration at the  $n$ th sampling point,  $V_0$  is the total volume of dialysis solution,  $V$  is the volume of sample taken out for analysis.

## 2.6 Characterization

The morphology of GO, GQDs, MSN-NH<sub>2</sub> and GQDs-MSN were evaluated using transmission electron microscopy (TEM). The morphology and thickness of GO and GQDs were performed using an atomic force microscope (AFM). The size distribution of GQDs were analysed using a dynamic light scattering (DLS). The features of MSN-NH<sub>2</sub> and GQDs-MSN were observed using a scanning electron microscope (SEM) with energy dispersive spectroscopy (SEM-EDS) under an accelerating voltage of 20 kV. Fourier-transform infrared (FT-IR) spectroscopy was used to study the chemical composition of the as-prepared MSN-NH<sub>2</sub> and GQDs-MSN. X-ray diffraction (XRD) patterns were obtained on a Bruker D8 Advance X-ray diffractometer with Cu K $\alpha$  radiation ( $\lambda = 0.15$ ), at accelerating voltage and current of 40 kV and 40 mA, respectively. The fluorescence spectra were obtained using a LS-55 spectrophotometer. The UV-vis spectra were measured using an Evolution-300 spectrophotometer with a quartz cell of 1 cm path length.

## 3 Results and discussion

### 3.1 Characterization of GQDs-MSN

Fig. 1 shows typical microscopy of the GO and GQDs. Fig. 1a presents a TEM image of GO, exhibiting folded features of transparent thin layer with non-uniform morphology. More detailed AFM (Fig. 1b) shows as-synthesized GO of 1-2 nm in thickness. This was proved as characteristic of a single or two layered sheets according to the previous reports.<sup>26,27</sup> GQDs appear as granular structure with homogeneous morphology (Fig. 1c) and the diameters of GQDs are mainly distributed in the range of 22-36 nm based on dynamic light scattering (DLS) (Fig. 1c, top right histogram). AFM images of the GQDs (Fig. 1d) shows that the topographic heights are between 1 and 2 nm, indicating that the GQDs are single layered or bi-layered.<sup>28,29</sup> Consequently, it can be concluded that the large graphene oxide sheets were successfully cut into small GQDs by the solvothermal cutting method.

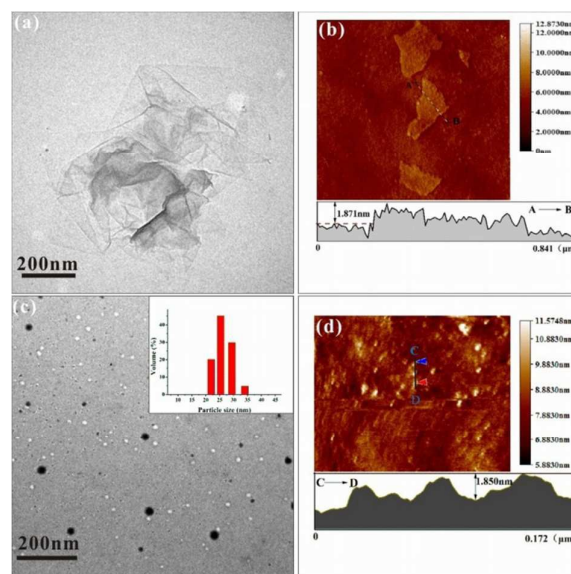


Fig. 1 The morphology and structure of GO and GQDs. TEM images of GO (a), AFM images and height profile along the line A-B of GO (b); TEM images and lateral size distribution (top right histogram) of GQDs (c), AFM images and height profile along the line C-D of GQDs (d).

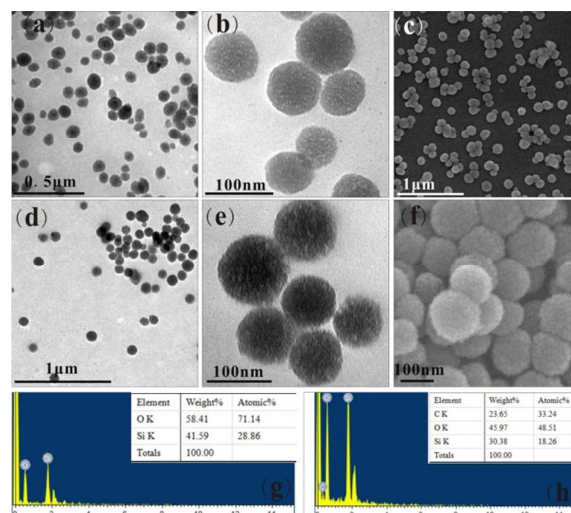


Fig. 2 The morphology and structure of MSN-NH<sub>2</sub> and GQDs-MSN. TEM images of MSN-NH<sub>2</sub> at different magnification (a, b), and SEM images of MSN-NH<sub>2</sub> (c); TEM images of GQDs-MSN at different magnification (d, e), and SEM images of GQDs-MSN (f); EDS for MSN-NH<sub>2</sub> (g) and GQDs-MSN (the mass ratio of GQDs/MSN is 8%) (h).

Fig. 2 shows the TEM and SEM-EDS images of the as-prepared MSN-NH<sub>2</sub> and GQDs-MSN. As shown in Fig. 2a-c, MSN-NH<sub>2</sub> consists of uniform spherical nanoparticles with diameter of 80-100 nm. Identically, it can be seen that spherical GQDs-MSN were about 90-100 nm in the size with good dispersibility and excellent morphology (Fig. 2d-f), which means the GQDs did not significantly induce the morphological changes as well as the particle size. In addition, it can be clearly observed that there is a strawberry-like structure on the surface of MSN-NH<sub>2</sub> (Fig. 2b), which indicated that the pure MSN possessed a mesoporous structure. The observed

downy-like over the entire surface of MSN-NH<sub>2</sub> are characteristic of GQDs, confirming the full adsorption of MSN-NH<sub>2</sub> by GQDs (Fig. 2e). Moreover, the chemical composition of MSN-NH<sub>2</sub> and GQDs-MSN were investigated using EDS elemental analysis. It can be seen that the element of Si (41.59%) and O (58.41%) are in the majority in MSN-NH<sub>2</sub> (Fig. 2g). Compared with the EDS spectrum of MSN, the GQDs-MSN showed a new C peak (23.65%), and the Si and O element decreased to 30.35% and 45.97% respectively (Fig. 2h), confirming the existence of GQDs on the surface of MSN-NH<sub>2</sub>. In addition, the strongly electrostatic interaction between oppositely charged MSN-NH<sub>2</sub> and GQDs together with the flexibility of GQDs can be responsible for the formation of the unique GQDs-MSN structure.<sup>30,31</sup>

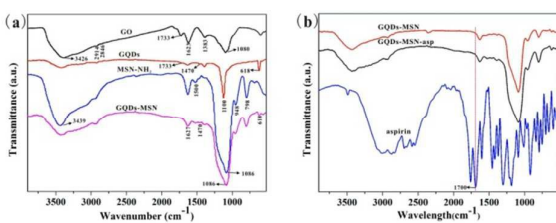


Fig. 3 FT-IR spectra of GO, GQDs, MSN-NH<sub>2</sub>, GQDs-MSN (a); and GQDs-MSN, GQDs-MSN-asp, aspirin (b).

Fig. 3a displays the FT-IR spectra of GO, GQDs, MSN-NH<sub>2</sub>, GQDs-MSN. The spectrum of GO is in good agreement with previous work.<sup>32</sup> The peak at 3426 cm<sup>-1</sup>, 1733 cm<sup>-1</sup> and 1623 cm<sup>-1</sup> were ascribed to the -OH vibration stretching, stretching of the C=O bond of carboxyl groups, and C=C bond, respectively. The bands at 2914 cm<sup>-1</sup> and 2846 cm<sup>-1</sup> were ascribed to the vibration of C-H, and the bands at around 1383 cm<sup>-1</sup> and 1080 cm<sup>-1</sup> were ascribed to the vibration of C-O. After the solvothermal treatment of the GO, the vibrational absorption band of C=O at 1733 cm<sup>-1</sup> became very weak, the bands about 1100 cm<sup>-1</sup> and 618 cm<sup>-1</sup> were ascribed to the vibration of C-N, and a new band displayed at 1470 cm<sup>-1</sup> was ascribed to N-H in-plane stretching of the amide group. These results confirmed that the DMF acted as the solvent as well as a weak reduction agent during the hydrothermal reaction. The large GO was cut and reduced simultaneously, and thus the GQDs were obtained. The MSN-NH<sub>2</sub> was validated by the asymmetrical and symmetrical stretching vibration of Si-O-Si (as: 1086 cm<sup>-1</sup>; s: 798 cm<sup>-1</sup>), and the bands at 948 cm<sup>-1</sup> was ascribed to the stretching vibration of Si-OH.<sup>33</sup> Additionally, the broad peak centered around 3439 cm<sup>-1</sup> was ascribed to O-H stretching vibrations of hydrogen-bonded surface silanol groups and physically adsorbed water. The peak at 1627 cm<sup>-1</sup> and 1500 cm<sup>-1</sup> were ascribed to the H-O-H bending vibrations of physically adsorbed water and the N-H vibration stretching, respectively, suggesting that MSN-NH<sub>2</sub> was successfully synthesized by the above method. Compared with MSN-NH<sub>2</sub>, the appearance of a new weak peak was located at 1470 cm<sup>-1</sup> and 618 cm<sup>-1</sup>, which were ascribed to the N-H stretching vibration and C-N stretching vibration, respectively. These results confirmed that the effective decoration of GQDs onto the surface of the MSN-NH<sub>2</sub>.

Fig. 4 shows the X-ray diffraction (XRD) of GO, GQDs, MSN-NH<sub>2</sub> and GQDs-MSN. The peak at 2 $\theta$  = 10.2° was corresponded to the (002) planes of GO.<sup>34</sup> The as-prepared GQDs shows a weak broad peak at 2 $\theta$  = 24.5°, which was attributed to the thinness and disordered stacking of some GQDs. In addition, there were some impurity peaks (2 $\theta$ =27.6°, 32.8° and 43.3°), suggesting that the GQDs obtained by the solvothermal method consist of amorphous form. It reveals a broad reflection profiles centered at 23°, ascribing to the MSN-NH<sub>2</sub>.<sup>35</sup> GQDs-MSN showed similar pattern with MSN-NH<sub>2</sub> at peak of 23° and did not exhibited any peaks of GQDs, demonstrating that MSN-NH<sub>2</sub> nanovehicles prevented the restacking of most GQDs attached.

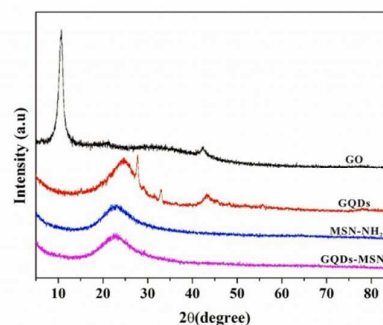


Fig. 4 XRD spectra of GO (a), GQDs (b), MSN-NH<sub>2</sub> (c) and GQDs-MSN (e).

### 3.2 properties of GQDs-MSN

Fig. 5 shows the N<sub>2</sub> adsorption and desorption isotherms and pore size distribution of the as-prepared of MSN-NH<sub>2</sub> and GQDs-MSN. As shown in Fig. 5a, the isotherm of MSN-NH<sub>2</sub> can be classified as type IV isotherms characteristic of mesoporous materials. The single point surface area at P/Po = 0.20 is 402.81 m<sup>2</sup>/g. The corresponding pore size distribution calculated from the adsorption branch of the nitrogen isotherm (inset of Fig. 5a) by BJH method shows a narrow pore size distribution peak at 4.40 nm, and the single point adsorption total pore volume of pores less than 69.28 nm diameter at P/Po = 0.97 is 0.47 cm<sup>3</sup>/g. In Fig. 5b, N<sub>2</sub> adsorption-desorption isotherms of GQDs-MSN also shows a typical type IV curve with a specific surface area of 640.82 m<sup>2</sup>/g, an average pore diameter of 4.02 nm, and the total pore volume of pores is 0.70 cm<sup>3</sup>/g. In addition, the specific surface area and total pore volume of pores were increased obviously and the average pore diameter were scarcely decreased, which could be ascribed to that fact that the pore depth increased upon the attachment of GQDs on the surface of MSN-NH<sub>2</sub> by electrostatic interaction. These result shows that the as-synthesized GQDs-MSN with mesoporous structures and high surface area may possess high drug loading capacity as drug carriers.

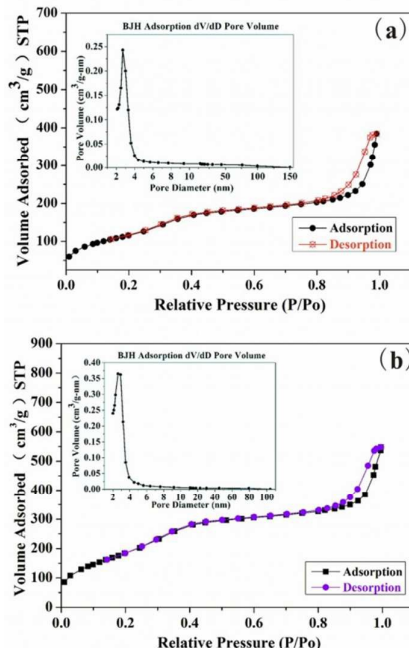


Fig. 5 N<sub>2</sub> adsorption/desorption isotherms of MSN-NH<sub>2</sub> (a) and GQDs-MSN (b), insets show the corresponding plots of pore size distribution from adsorption curve.

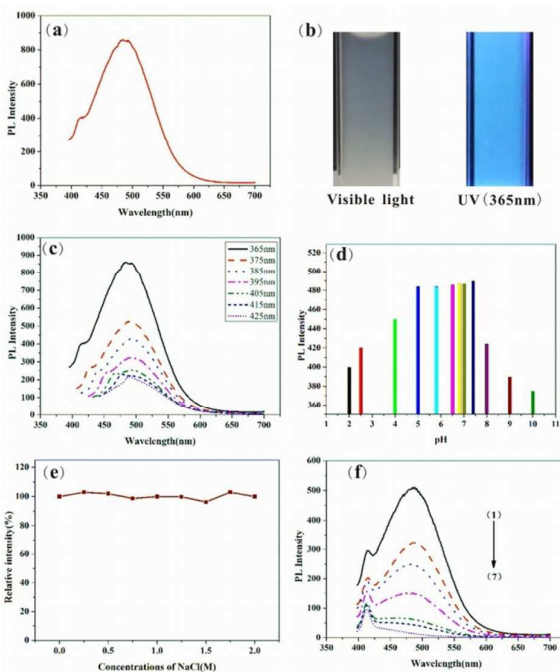


Fig. 6 The optical properties of GQDs-MSN. Fluorescence spectra of GQDs-MSN excited at 365 nm (a); Photograph of the GQDs-MSN ethanol solution taken under visible light and 365 nm UV light, from left to right, respectively (b); The excitation-dependent PL behavior of GQDs-MSN (c); Effect of pH on the fluorescence intensity of GQDs-MSN (d); Effect of ionic strengths (different concentrations of NaCl) on the fluorescence intensity of GQDs-MSN (e); Emission spectra of GQDs-MSN in ethanol at various concentrations: (1)  $1.0 \times 10^{-3}$  mg/mL, (2)  $1.0 \times 10^{-4}$  mg/mL, (3)  $1.0 \times 10^{-5}$  mg/mL, (4)  $1.0 \times 10^{-6}$  mg/mL, (5)  $1.0 \times 10^{-7}$  mg/mL, (6)  $1.0 \times 10^{-8}$  mg/mL, (7) ethanol.

Fig. 6 reveals the optical properties of the as-prepared GQDs-MSN. As shown in Fig. 6(a, b), the GQDs-MSN ethanol suspension exhibits strong blue fluorescence under UV excitation (365 nm) which can be easily seen with the naked eye and the emission peak located at 490 nm. The ethanol solution of GQDs-MSN exhibited an excitation dependent PL behavior (Fig. 6c). As it was excited at wavelengths from 365 to 425 nm, the emission peak shifted from 487 nm to 506 nm and its intensity decreased obviously. In addition, an interesting phenomenon is its pH-dependent photoluminescence property (Fig. 6d). Fluorescence intensity of the GQDs-MSN decreased in a solution of low or high pH, but maintained high intensity in a solution of pH 5-7.5, which was ascribed to the fact that moderated pH has the advantage of electrostatic interaction formation between amino and carboxyl groups. Another interesting phenomenon is that the fluorescence properties of the as-obtained GQDs-MSN at different ionic strengths remain constant when increasing the concentration of NaCl from 0 to 2.0 M (Fig. 6e). To further explore the photoluminescence properties of the as-obtained GQDs-MSN, the photoluminescence spectra of the GQDs-MSN was measured in ethanol solutions at different concentrations (Fig. 6f). The PL intensity of GQDs-MSN decreased as the concentration of GQDs-MSN decreased, but the location of the emission peak remain constant and did not appear any new emission peaks, which indicated that the as-obtained GQDs-MSN were monodisperse in ethanol solution.<sup>36</sup> Therefore, the GQDs-MSN is a better candidate as a fluorescence label for bioimaging due to these excellent photoluminescence properties.

### 3.3 Performances of GQDs-MSN for aspirin loading and release

To explore the capability of the GQDs-MSN as a drug carrier vehicles, aspirin, an efficient anti-platelet drug, was used as a model drug. Fig. 3b shows the FT-IR spectra of aspirin and the GQDs-MSN nanohybrid before and after loading aspirin. After loading the GQDs-MSN with aspirin, almost no changes were observed in the FT-IR spectra due to the overlapping vibrational bands of the MSN-NH<sub>2</sub> and aspirin. The C=O vibration at  $1700 \text{ cm}^{-1}$  was almost disappeared, which was attributed to the strong interaction of the carbonyl carbon of the carboxylic acid with the amine groups to the formation of a carboxylate species,<sup>37</sup> suggesting that aspirin successfully loaded on GQDs-MSN. The measurement using UV-vis absorbance spectroscopy and fluorescence spectrophotometer revealed the drug loading capacity and fluorescence intensity. As shown in Table 1, the drug loading capacities of GQDs-MSN increased as the mass ratio of GQDs/MSN increased, and the maximum drug loading is about 36.59% with the mass ratio of 8% for GQDs/MSN, which is twice as much as that of pure MSN. It is worth noting that the GQDs-MSN exhibits much higher aspirin loading capacity than the previously reported MSN-based NPs.<sup>38,39</sup> The high drug loading capacity was ascribed to the high specific surface area and total pore volume of pores, which was consistent with the results of N<sub>2</sub> adsorption-desorption analysis.

**Table 1** Drug loading capacity and fluorescence intensity of GQDs-MSN with different mass ratio of GQDs/MSN

GQDs/MSN (% w/w)	0	0.1	0.5	1	4	8	16	20
aspirin loading (% w/w)	18.26	31.90	32.37	35.12	36.07	36.59	30.79	30.00
fluorescence intensity	0	281.31	226.13	243.70	318.08	361.01	415.84	667.97

An excellent drug carrier should possess the capacity to load and controlled-release drug molecules. Fig. 7 shows the aspirin release from aspirin-loaded GQDs-MSN over a 33 h period in PBS with different pH values (2.5, 5.0 and 7.4) at 37 °C, respectively. The aspirin loaded GQDs-MSN has sustained release property, and the aspirin release rate decreases with the increase in pH values (from 2.5 to 7.4). With the decrease of pH, more and more of the loaded aspirin molecules were protonized, resulting in aspirin release from the drug carrier, and about 95.15% of the loaded aspirin was released at pH=2.5 within 33 h, while only 66.31% of it was released at pH=7.4 at the same time. These results undoubtedly demonstrated that the GQDs-MSN as a drug carrier have a pH-triggered release property for loaded-aspirin.

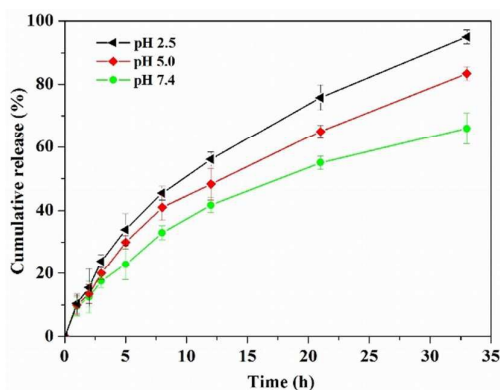


**Fig. 7** The release of aspirin on GQDs-MSN at different pH values, all the experiments were repeated three times for the calculation of standard deviation.

## Conclusions

In summary, fluorescent GQDs-MSN through electrostatic interaction were successfully synthesized, and the aspirin loading capacity and pH-dependent release behavior were investigated thereafter. The aspirin loading capacity could reach 36.59% (mg/mg), which is twice as much as pure MSN-NH<sub>2</sub>, and is superior to the conventional MSN-related materials. Importantly, the *in vitro* assay showed the release of aspirin from the aspirin-loaded GQDs-MSN was pH-dependent, and approximately 95.15% of the loaded aspirin was released at pH of 2.5 within 33 h. This result makes the system reported here a potential candidate in the formulation of a pH-sensitive vehicle for *in vivo* delivery of therapeutic agents to low pH tissues, such as tumors and inflammatory sites. Moreover, in view of the excellent photoluminescent property and efficient

drug release properties, these nanocomposites are expected to achieve integration of tumor diagnosis and treatment.

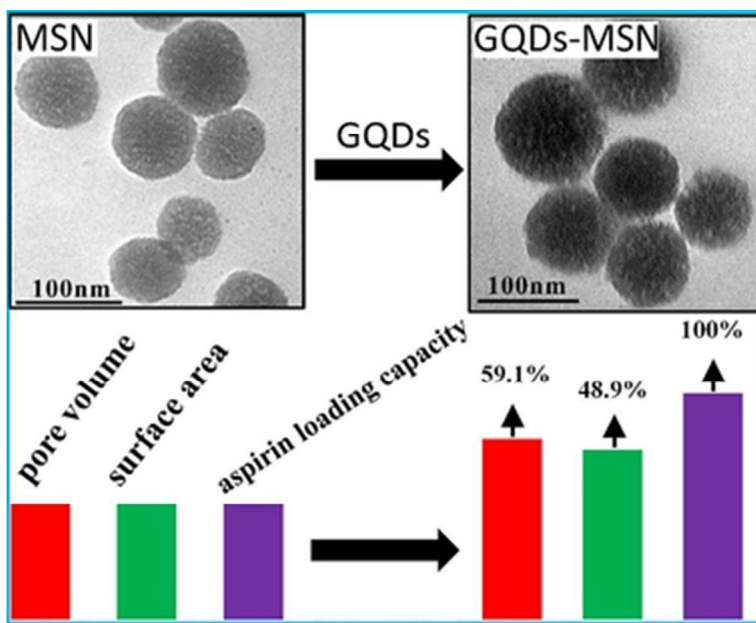
## Acknowledgements

This work was supported by the Natural Science Foundation of Hubei (Program No. 2011CDC068), the State Key Laboratory of Agricultural Microbiology (Program No. AMLKF201205), and the Fundamental Research Funds for the Central Universities (Program No. 52902-0900202265 and 2662015PY153).

## References

- 1 A. Popat, B. P. Ross, J. Liu, S. Jambhrunkar, F. Kleitz, and S. Z. Qiao, *Angew. Chem. Int. Ed.*, 2012, **51**, 12486–12489.
- 2 Q. J. He and J. L. Shi, *J. Mater. Chem.*, 2011, **21**, 5845–5855.
- 3 C. R. Thomas, D. P. Ferris, J. H. Lee, E. Choi, M. H. Cho, E. S. Kim, J. F. Stoddart, J. S. Shin, J. Cheon and J. I. Zink, *J. Am. Chem. Soc.*, 2010, **132**, 10623–10625.
- 4 A. Popat, S. B. Hartono, F. Stahr, J. Liu, S. Z. Qiao and G. Q. Lu, *Nanoscale*, 2011, **3**, 2801–2818.
- 5 I. I. Slowing, B. G. Trewyn, S. Giri and V. S. Y. Lin, *Adv. Funct. Mater.*, 2007, **17**, 1225–1236.
- 6 D. R. Radu, C.Y. Lai, K. Jeftinija, E. W. Rowe, S. Jeftinija and V. S. Y. Lin, *J. Am. Chem. Soc.*, 2004, **126**, 13216–13217.
- 7 J. E. Lee, N. Lee, H. Kim, J. Kim, S. H. Choi, J. H. Kim, T. Kim, I. C. Song, S. P. Park, W. K. Moon and T. Hyeon, *J. Am. Chem. Soc.*, 2010, **132**, 552–557.
- 8 D. Tarn, C. E. Ashley, M. Xue, E. C. Carnes, J. I. Zink and C. J. Brinker, *Acc. Chem. Res.*, 2013, **46**, 792–801.
- 9 M. Levitus and S. Ranjit, *Q. Rev. Biophys.*, 2011, **44**, 123–151.
- 10 P. H. Zhang, W. R. Huan, H. Xu, S. L. Chang, C. Cao, M. Q. Kong and Y. J. He, *Microporous Mesoporous Mater.*, 2014, **188**, 86–92.
- 11 A. M. Derfus, W. C. W. Chan and S. N. Bhatia, *Nano Lett.*, 2004, **4**, 11–18.
- 12 C. Kirchner, T. Liedl, S. Kudera, T. Pellegrino, A. M. Javier, H. E. Gaub, S. Stölzle, N. Fertig and W. J. Parak, *Nano Lett.*, 2005, **5**, 331–338.
- 13 D. A. Limaye and Z. A. Shaikh, *Toxicol. Appl. Pharmacol.*, 1999, **154**, 59–66.
- 14 M. Kondoh, S. Araragi, K. Sato, M. Higashimoto, M. Takiguchi and M. Sato, *Toxicology*, 2002, **170**, 111–117.
- 15 K. S. Novoselov, A. K. Geim, S. V. Morozov, D. Jiang, Y. Zhang, S. V. Dubonos, I. V. Grigorieva and A. A. Firsov, *Science*, 2004, **306**, 666–669.
- 16 L. Liao, H. L. Peng and Z. F. Liu, *J. Am. Chem. Soc.*, 2004, **136**, 12194–12200.
- 17 Y. Wang, Z. H. Li, D. H. Hu, C. T. Lin, J. H. Li and Y. H. Lin, *J. Am. Chem. Soc.*, 2012, **132**, 9274–9276.
- 18 J. Peng, W. Gao, B. K. Gupta, Z. Liu, R. Romero-Aburto, L. H. Ge, L. Song, L. B. Alemany, X. B. Zhan, G. H. Gao, S. A. Vithayathil, B. A. Kaiparettu, A. A. Marti, T. Hayashi, J. J. Zhu and P. M. Ajayan, *Nano Lett.*, 2012, **12**, 844–849.
- 19 J. H. Shen, Y. H. Zhu, X. L. Yang and C. Z. Li, *Chem. Commun.*, 2012, **48**, 3686–3699.
- 20 V. Gupta, N. Chaudhary, R. Srivastava, G. D. Sharma, R. Bhardwaj and S. Chand, *J. Am. Chem. Soc.*, 2011, **133**, 960–9963.
- 21 X. M. Sun, Z. Liu, K. Welscher, J. T. Robinson, A. Goodwin, S. Zaric and H. J. Dai, *Nano Res*, 2008, **1**, 203–212.
- 22 Y. Q. Dong, G. L. Li, N. N. Zhou, R. X. Wang, Y. W. Chi and G. N. Chen, *Anal. Chem.*, 2012, **84**, 8378–8382.
- 23 Q. Liu, B. D. Guo, Z. Y. Rao, B. H. Zhang and J. R. Gong, *Nano Lett.*, 2013, **13**, 2436–2441.

- 1  
2  
3  
4  
5  
6  
7  
8  
9  
10  
11  
12  
13  
14  
15  
16  
17  
18  
19  
20  
21  
22  
23  
24  
25  
26  
27  
28  
29  
30  
31  
32  
33  
34  
35  
36  
37  
38  
39  
40  
41  
42  
43  
44  
45  
46  
47  
48  
49  
50  
51  
52  
53  
54  
55  
56  
57  
58  
59  
60
- 24 S. M. Zhang, H. Y. Zhang, Q. Liu and S. L. Chen, *J. Mater. Chem. A*, 2013, **1**, 3302–3308.
- 25 S. J. Zhu, J. H. Zhang, C. Y. Qiao, S. J. Tang, Y. F. Li, W. J. Yuan, B. Li, L. Tian, F. Liu, R. Hu, H. N. Gao, H. T. Wei, H. Zhang, H. C. Sun and B. Yang, *Chem. Commun.*, 2011, **47**, 6858–6860.
- 26 L. Zhang, X. Li, Y. Huang, Y. F. Ma, X. J. Wan and Y. S. Chen, *Carbon*, 2010, **48**, 2361–2380.
- 27 J. P. Zhao, S. F. Pei, W. C. Ren, L. B. Gao and H. M. Cheng, *ACS Nano*, 2010, **4**, 5245–5252.
- 28 D. Y. Pan, J. C. Zhang, Z. Li and M. H. Wu, *Adv. Mater.*, 2010, **22**, 734–738.
- 29 Y. Q. Dong, C. Q. Chen, X. T. Zheng, L. L. Gao, Z. M. Cui, H. B. Yang, C. X. Guo, Y. W. Chi and C. M. Li, *J. Mater. Chem.*, 2012, **22**, 8764–8766.
- 30 T. Chen, H. Yu, N. W. Yang, M. D. Wang, C. D. Ding and J. J. Fu, *J. Mater. Chem. B*, 2014, **2**, 4979–4982.
- 31 L. Zhou, Z. H. Li, Z. Liu, J. S. Ren and X. G. Qu, *Langmuir*, 2013, **29**, 6396–6403.
- 32 X. Y. Yang, X. Y. Zhang, Z. F. Liu, Y. F. Ma, Y. Huang and Y. S. Chen, *J. Phys. Chem. C*, 2008, **112**, 17554–17558.
- 33 W. X. Sun, W. Z. Sun, M. R. Kessler, N. Bowler, K. W. Dennis, R. W. McCallum, Q. Li and X. L. Tan, *ACS Appl. Mater. Interfaces*, 2013, **5**, 1636–1642.
- 34 H. Q. Wu, B. B. Tang and P. Y. Wu, *J. Membr. Sci.*, 2014, **451**, 94–102.
- 35 H. W. Gu, Y. B. Guo, S. Y. Wong, Z. Zhang, X. P. Ni, Z. X. Zhang, W. X. Hou, C. H. He, V. P. W. Shim and X. Li, *Microporous Mesoporous Mater.*, 2013, **170**, 226–234.
- 36 D. Nagao, N. Anzai, Y. Kobayashi, S. C. Gu and M. Konno, *J. Colloid Interface Sci.*, 2006, **298**, 232–237.
- 37 A. Datt, I. El-Maazawi and S. C. Larsen, *J. Phys. Chem. C*, 2012, **116**, 18358–18366.
- 38 Y. F. Zhu, E. Kockrick, T. Ikoma, N. Hanagata and S. Kaskel, *Chem. Mater.*, 2009, **21**, 2547–2553.
- 39 J. L. Pang, X. Y. Li, G. W. Zhou, B. Sun and Y. Q. Wei, *RSC Adv.*, 2015, **5**, 6599–6606.



32x26mm (300 x 300 DPI)